AIP | Review of Scientific Instruments

An apparatus for studying electrical breakdown in liquid helium at 0.4 K and testing electrode materials for the neutron electric dipole moment experiment at the Spallation Neutron Source

T. M. Ito, J. C. Ramsey, W. Yao, D. H. Beck, V. Cianciolo, S. M. Clayton, C. Crawford, S. A. Currie, B. W. Filippone, W. C. Griffith, M. Makela, R. Schmid, G. M. Seidel, Z. Tang, D. Wagner, W. Wei, and S. E. Williamson

Citation: Review of Scientific Instruments **87**, 045113 (2016); doi: 10.1063/1.4946896
View online: http://dx.doi.org/10.1063/1.4946896
View Table of Contents: http://scitation.aip.org/content/aip/journal/rsi/87/4?ver=pdfcov
Published by the AIP Publishing

An apparatus for studying electrical breakdown in liquid helium at 0.4 K and testing electrode materials for the neutron electric dipole moment experiment at the Spallation Neutron Source

T. M. Ito,[1,a)] J. C. Ramsey,[1] W. Yao,[2] D. H. Beck,[3] V. Cianciolo,[2] S. M. Clayton,[1] C. Crawford,[4] S. A. Currie,[1] B. W. Filippone,[5] W. C. Griffith,[1] M. Makela,[1] R. Schmid,[5] G. M. Seidel,[6] Z. Tang,[1] D. Wagner,[4] W. Wei,[1] and S. E. Williamson[3]
[1]*Los Alamos National Laboratory, Los Alamos, New Mexico 87545, USA*
[2]*Oak Ridge National Laboratory, Oak Ridge, Tennessee 37831, USA*
[3]*Loomis Laboratory of Physics, University of Illinois, Urbana, Illinois 61801, USA*
[4]*Department of Physics and Astronomy, University of Kentucky, Lexington, Kentucky 40506, USA*
[5]*W. K. Kellogg Radiation Laboratory, California Institute of Technology, Pasadena, California 91125, USA*
[6]*Department of Physics, Brown University, Providence, Rhode Island 02912, USA*

(Received 20 October 2015; accepted 2 April 2016; published online 25 April 2016)

We have constructed an apparatus to study DC electrical breakdown in liquid helium at temperatures as low as 0.4 K and at pressures between the saturated vapor pressure and ~600 Torr. The apparatus can house a set of electrodes that are 12 cm in diameter with a gap of 1–2 cm between them, and a potential up to ±50 kV can be applied to each electrode. Initial results demonstrated that it is possible to apply fields exceeding 100 kV/cm in a 1 cm gap between two electropolished stainless steel electrodes 12 cm in diameter for a wide range of pressures at 0.4 K. We also measured the current between two electrodes. Our initial results, $I < 1$ pA at 45 kV, correspond to a lower bound on the effective volume resistivity of liquid helium of $\rho_V > 5 \times 10^{18}$ Ω cm. This lower bound is 5 times larger than the bound previously measured. We report the design, construction, and operational experience of the apparatus, as well as initial results. *Published by AIP Publishing.* [http://dx.doi.org/10.1063/1.4946896]

I. INTRODUCTION

A nonzero permanent electric dipole moment (EDM) of a nondegenerate state of a system with spin $J \neq 0$ violates invariance under time reversal as well as invariance under parity operation. The violation of time reversal invariance implies a violation of invariance under CP operation (combined operations of parity and charge conjugation) through the CPT theorem.

Searches for new sources of CP violation through searches of EDM are strongly motivated for the following reasons: (1) The amount of CP violation contained in the Standard Model (SM) of particle physics through the complex phase of the Cabibbo-Kobayashi-Maskawa (CKM) matrix is known to be insufficient for generating the observed matter-antimatter asymmetry in the Universe (therefore it is expected that there are other sources of CP violation). (2) The other source of CP violation contained in the SM, the so-called θ term in the quantum chromodynamics (QCD) Lagrangian, is constrained by nonobservation of the neutron EDM (nEDM) to be unnaturally small. (3) The SM value of EDMs based on the CKM phase is highly suppressed because in the SM the CP violation processes are quark flavor-changing at the tree level. (4) Many extensions of the SM contain new sources of CP violation, predicting much larger values of EDMs.

The search for the neutron EDM (nEDM) was pioneered by Smith *et al.*[1] In the subsequent 60 odd years, many more experiments have been performed with increasingly refined experimental methods and with correspondingly improved sensitivities and upper limits. (For a review of experimental searches for the nEDM, see, e.g., Ref. 2.) Many of these experiments have looked for the nEDM by subjecting spin polarized neutrons to static magnetic and electric fields and looking for the possible change in the spin precession frequency corresponding to the change in the relative orientation of the electric field with respect to the magnetic field. Whereas early experiments were performed using a beam of cold neutrons, all recent experiments have used stored ultracold neutrons (UCNs)[3,4] to suppress the effect of the motional magnetic field[2] (see, however, Ref. 5).

The statistical sensitivity of such measurements for a batch of stored UCNs depends on three quantities, namely, E the strength of the electric field, T the free precession time, and N the number of neutrons in the batch and is expressed as follows:

$$\delta d_n \propto \frac{1}{ET\sqrt{N}}. \quad (1)$$

Typically many such measurements are repeated over the duration of an experiment. The current limit, given by an experiment performed at Institut Laue Langevin by a group led by the University of Sussex, is $d_n < 2.9 \times 10^{-26}$ e cm (90% C.L.).[6] (A recent updated analysis gives $d_n < 3.0 \times 10^{-26}$ e cm (90%

a)Author to whom correspondence should be addressed. Electronic mail: ito@lanl.gov

C.L.).[7]) In this experiment, typical values for E, T, and N were $E = 10$ kV/cm, $T = 130$ s, and $N = 14\,000$.

A new nEDM experiment, to be mounted at the Fundamental Neutron Physics Beamline (FnPB)[8] at the Spallation Neutron Source (SNS) at Oak Ridge National Laboratory, is currently being developed with a sensitivity goal of $\delta d_n \sim 3 \times 10^{-28}$ e cm.[9,10] This experiment is based on the method proposed by Golub and Lamoreaux.[11] In this method, the experiment is performed inside a bath of liquid helium (LHe) at approximately 0.4 K. The unique features of this experiment include the following:

1. *In situ* production of UCNs inside the measurement cells from a cold neutron beam of 0.89 nm wavelength using the superthermal process in superfluid liquid helium.[12]
2. Use of spin-polarized ^{3}He atoms as a comagnetometer.
3. Use of the spin-dependent neutron capture reaction on a ^{3}He atom ($n+^3\mathrm{He} \rightarrow p + t$) and resulting LHe scintillation (see, e.g., Ref. 13) as the analyzer of the neutron spin.

With this method, we expect to increase all of E, T, and N in Eq. (1) significantly over the previous experiments. LHe is expected to be a better insulator than vacuum. In addition, processes responsible for electrical breakdown initiated at the electrode-insulator junction, thought to be one of the factors limiting the achievable electric field strength for previous room temperature nEDM experiments, are expected to be suppressed in LHe. Therefore a larger E can be expected. Performing a measurement at cryogenic temperatures suppresses some of the loss mechanisms for stored UCNs, resulting in longer T.[14,15] Producing UCNs directly in the experiment from a 0.89 nm cold neutron beam is expected to provide a larger N.

Of critical importance to the development of this experiment is to establish the highest electric field that can be applied and be sustained stably in the volume inside the measurement cells because the sensitivity of the experiment directly depends on the strength of the applied electric field.

As part of the research and development (R&D) for the SNS nEDM experiment, we have constructed an apparatus to study DC electrical breakdown in LHe at temperatures as low as 0.4 K and at pressures between the saturated vapor pressure (SVP) and ~600 Torr. In this paper, we describe the design, construction, and operational experience of this apparatus. We also report the initial findings.

The rest of this paper is organized as follows. In Sec. II, the electric field requirements for the SNS nEDM experiment will be reviewed. After a brief review of the current understanding of phenomenon of electrical breakdown in LHe in Sec. III, the purpose of the new high voltage (HV) testing apparatus will be discussed and an overview of its design will be given in Sec. IV. The details of the cryogenic design of the apparatus will be given in Sec. V, whereas the design of the HV components will be discussed in Sec. VI. The cryogenic performance of the apparatus, as well as our operational experience with cryogenic aspects of the apparatus, will be discussed in Sec. VII. The HV performance, our operational experience with HV aspects of the apparatus, and some initial HV results will be presented in Sec. VIII. Section IX will give a summary of this paper.

II. ELECTRIC FIELD REQUIREMENTS FOR THE SNS NEDM EXPERIMENT

The design goal for the SNS nEDM experiment is to have an electric field of 75 kV/cm stably applied in the volume inside the so-called measurement cells, the volumes filled with 0.4 K LHe that stores UCNs. The measurement cell walls will be made of poly(methyl methacrylate) (PMMA), as they will serve as part of the light collection system. They will be 10.16 cm × 12.70 cm × 42 cm in outer dimension with a wall thickness of 1.2 cm. The two measurement cells will be sandwiched between electrodes, roughly 10 cm × 40 cm × 80 cm in size. The electrodes and the measurement cells will be immersed in 0.4 K LHe.

There are a number of requirements on the electrode materials. They are as follows:

1. In order to match the thermal contraction of the measurement cells made of PMMA, which shrinks ~1% when cooled from room temperature to 0.4 K, the electrodes need to be made of a material that has similar thermal contraction characteristics to PMMA. The current design is to use PMMA as the electrode substrate material and make the electrode surface conducting using methods including (1) coating with appropriate materials and (2) implanting conducting materials into the surface layer.
2. The material cannot have too high an electrical conductivity. This requirement comes from the requirement on Johnson noise on the superconducting quantum interference device (SQUID)-based magnetometer to measure the precession frequency of spin polarized ^{3}He atoms and also from the requirement on Joule heating from eddy currents due to the radio frequency (RF) field for dressed spin measurement.[11] The allowed surface resistivity is $100\ \Omega/\square < \sigma < 10^8\ \Omega/\square$ at the operating temperature of ~0.4 K.
3. The material should be non-magnetic. The static magnetic field in the region inside the measurement cells, which is approximately 1 μT, needs to be uniform to 5×10^{-4} and needs to have field gradients smaller than 5 pT/cm in the direction of the static field and 10 pT/cm in the direction perpendicular to the static field. Because of this stringent requirement, many of the so-called "non-magnetic" technical materials, such as stainless steel and inconel, are disallowed. Also, materials that become superconducting cannot be used because the field expelled due to the Meissner effect would disturb the field uniformity inside the measurement cells.
4. The material should not have large neutron absorption properties, as such materials would become radioactively activated due to the exposure to a high flux neutron beam and become source of background radiation.

The current candidate methods for making the PMMA electrode surface conducting include graphite paint and copper ion implantation.

In addition, the leakage currents along the cell walls need to be minimized. This requirement comes from the following considerations.

- These currents produce magnetic fields that are correlated with the direction of the electric field and therefore can produce effects that mimic the signal of nEDM (this applies to all nEDM experiments that use stored UCN).
- In the current design, the necessary HV will be generated inside the LHe volume using a gain capacitor. In this method, the nEDM experiment will be run with the HV electrode disconnected from the HV power supply. Leakage currents lead to a reduction of the electric field over time.
- These currents produce heat, generating phonons in superfluid LHe and modifying the spatial distribution of the ^{3}He atoms via the ^{3}He-phonon interactions.

A schematic of the central part of the SNS nEDM experiment, as it is currently designed, is shown in Fig. 1.

III. ELECTRICAL BREAKDOWN IN LIQUID HELIUM

Electrical breakdown in liquid helium has been studied extensively[16] because of its importance in cooling superconducting components, principally high field magnets. In general, the experimental measurements of breakdown show little consistency, varying with geometry, electrode material, bubble formation, and unexplained parameters.

An electron with low kinetic energy forms a bubble in liquid helium. Because of the overlap with the electrons of the helium atoms, a free electron has a lower energy by close to an eV compared to that when it is in the conduction band. The radius of the bubble is about 19 Å. In a high electric field, an electron does not escape the bubble. Its motion is constrained by viscous damping or in the superfluid state by the creation of vortex rings or rotons, depending on pressure. In contrast, because of electrostriction, positive He ions form solid-like structures with surrounding atoms called "snowballs." The kinetic energy of a snowball in an electric field is also limited by damping and vortex ring creation. Neither electron bubbles nor positive ion snowballs can be the source of breakdown in liquid helium.

An electron created in the conduction band in a high electric field, on the other hand, can in principle lead to breakdown by electron impact ionization. However, the breakdown field of bulk liquid helium is calculated to be very high. The mean free path of a conduction electron, limited by elastic scattering from He atoms, is only about 100 nm and the ionization energy of He is 24.6 eV. Belevtsev[17] has made a detailed theoretical study of electron multiplication induced by an electric field in liquid helium starting from the kinetic Boltzmann equation. Taking into account the various electron energy loss mechanisms, he finds that the first Townsend coefficient reaches a value of 1 cm^{-1} at a field of 1.5 MV/cm rising to 102 cm^{-1} at 2.5 MV/cm. Hence, breakdown by electron impact ionization in any reasonable sized volume of helium can be expected to occur only at a field in the low MV/cm region, well above the fields of interest for this experiment.

Breakdown fields around or below 100 kV/cm have been commonly reported in the literature for liquid helium. These observations are presumed to be the result of phenomena occurring at the cathode. If the field emission of electrons on a rough surface can occur because of extremely high local fields at sharp asperities, local heating can result in vapor bubble formation leading to electron multiplication and vapor growth proceeding together. Breakdown is then the result of a vapor column extending to the anode. Note that in other dielectric liquids, formation and growth of vapor bubbles associated with electrical breakdown have been observed experimentally[18–20] (see also Ref. 21).

It follows that the parameters that can affect the breakdown field strength include (1) electrode material, in particular the surface properties and (2) LHe temperature and pressure

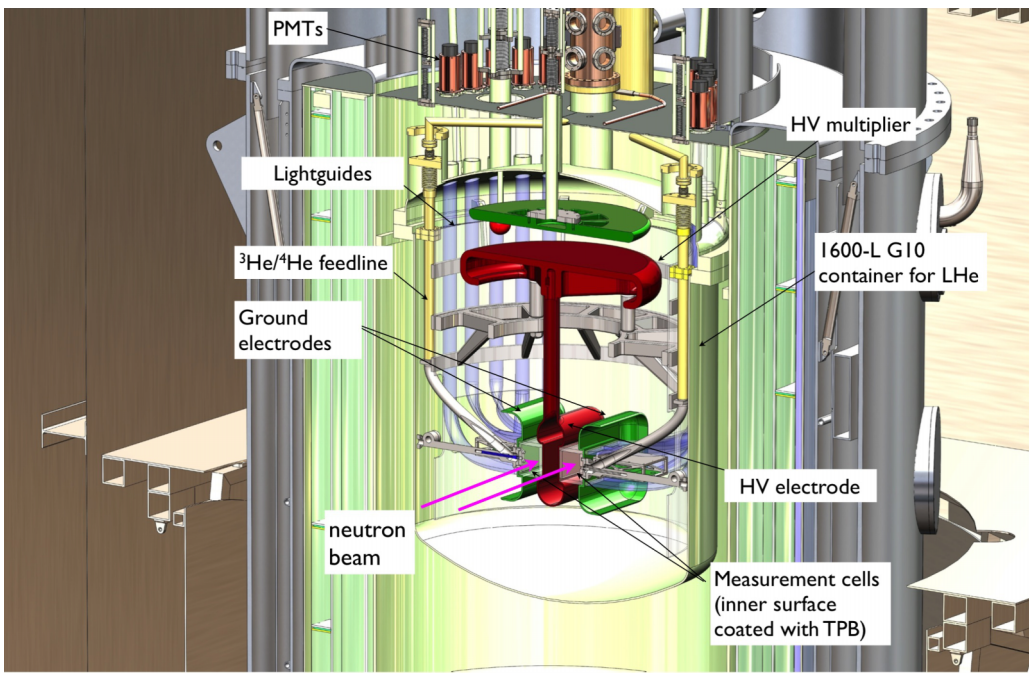

FIG. 1. A schematic of the central part of the SNS nEDM experiment, as it is currently designed.

(vapor growth can depend on the pressure). Note that LHe is unique among liquids in that its SVP changes drastically as a function of the temperature. For example, the SVP is 760 Torr at 4.2 K and is $\sim 10^{-6}$ Torr at 0.4 K.

In addition, because electrical breakdown is a stochastic process, the size of the system affects the breakdown field strength and its distribution, as shown in Ref. 22, in which the experimentally measured dependence of the breakdown field on the electrode surface area was shown to agree with a prediction based on the measured breakdown field distribution for electrodes of a particular size and the theory of extreme values, for the case in which transformer oil was used as insulator fluid.

In general, particles and other contamination in the liquid affect the electrical breakdown properties.[21] In the case of LHe, however, it is expected that they play a less important role because all possible contaminating species freeze at LHe temperature. Additionally solid particles (made of, e.g., metal) would most likely settle at the bottom of a container due to the low density of LHe ($\rho \sim 0.145$ g/cm^3 for $T < 2$ K).

IV. PURPOSE OF THE APPARATUS AND OVERVIEW OF THE DESIGN

The considerations given above indicate that the R&D for the SNS nEDM experiment requires a study of electrical breakdown in LHe in a condition (i.e., temperature, pressure, and size) close to that expected for the SNS nEDM experiment, using suitable electrode candidate materials.

It is also very important to study the effect of the presence of a dielectric insulator sandwiched between electrodes, as such will be the geometry for the SNS nEDM experiment. Note that even in a room temperature vacuum system, electric fields exceeding a few 100 kV/cm are possible when there is no insulator directly sandwiched between the two electrodes. In a study performed using a room temperature vacuum apparatus[23] similar to those used in the previous nEDM experiments (such as Ref. 6), the electric field was limited to ~30 kV/cm due to the presence of the UCN confining wall that was sandwiched between the two electrodes. (In the actual nEDM experiment, the achievable field was further lowered to $E \sim 10$ kV/cm due to other factors.) Field emission at the cathode-insulator junction is thought to be responsible for initiating breakdown,[24] which is temperature independent. However, we expect the processes responsible for leading field emission to breakdown to be suppressed in LHe.

In order to study the relevant aspects of electrical breakdown in LHe with a goal of establishing the feasibility of the SNS nEDM experiment as well as guiding the design of the apparatus, we constructed an apparatus called the Medium Scale HV (MSHV) test apparatus, which is described in this paper.

There are some important design aspects that required close attention to ensure that the apparatus yielded properly interpretable results. The inconsistencies seen in previous results may well have been partly due to lack of proper attention to these aspects.

One is proper electrostatic design. As discussed earlier, because electrical breakdown is a stochastic process, the size of the system affects the breakdown field strength and its distribution. It is therefore important to have a good understanding of the area of the electrodes that is exposed to high fields (and/or the size of the stressed dielectric volume) for proper interpretation of the results. For example, in a typical plane-to-plane geometry in which electrodes are made of a flat disk whose edge is rounded with a constant radius of curvature, it can be shown that the field is the highest where the flat surface connects to the rounded edge. If the distance between the two such electrodes is varied in order to study the gap size dependence of the breakdown field, one can be led to erroneous results because the ratio between the highest field and the field at the center of the electrodes increases as the gap size is increased. In order to study the breakdown field in a plane-to-plane geometry, so-called uniform field electrodes (UFEs) need to be used.

Another is proper heat management. Due to the rather low heat of vaporization of liquid helium (83 J/mol), a small amount of heat transmitted to the electrodes through HV feed lines can boil LHe on the electrode surfaces, creating bubbles and significantly reducing the breakdown field. It is, therefore, of critical importance to properly thermally anchor HV feed lines. Similarly, it is important to make sure that all components in the system are properly cooled before any measurements are taken. Performing breakdown field measurements before a sufficient amount of heat is removed from all the relevant components can lead to erroneous results due to boiling of LHe caused by residual heat in the system.

We used a ^{3}He refrigerator to cool the Central Volume (CV), the volume that contains LHe and houses electrodes to be tested, to the operating temperature of 0.4 K. The size of the CV was determined by striking a balance between the following two competing factors:

- Short turnaround time (time from the beginning of one cooldown to the beginning of the next) of the system (~2 weeks) to allow multiple electrode material candidates to be tested.
- Size large enough to give information relevant for the SNS nEDM experiment.

The chosen size of the CV holds 6 l of LHe, housing a set of electrodes 12 cm in diameter. The gap size is adjustable between 1 and 2 cm. Each dimension is within a factor of 5 or so of the SNS nEDM experiment's measurement cell electrodes.

Since we expect the pressure to be an important parameter affecting the breakdown field strength in LHe, the MSHV system is designed so that the pressure of the LHe volume in which the electrodes are placed can be varied between the SVP and ~600 Torr.

A schematic of the MSHV system is shown in Fig. 2.

V. CRYOGENIC DESIGN

As shown in Fig. 2, the MSHV cryostat consists of the following major components:

- Outer vacuum chamber (OVC), which separates the insulating vacuum from the atmosphere.

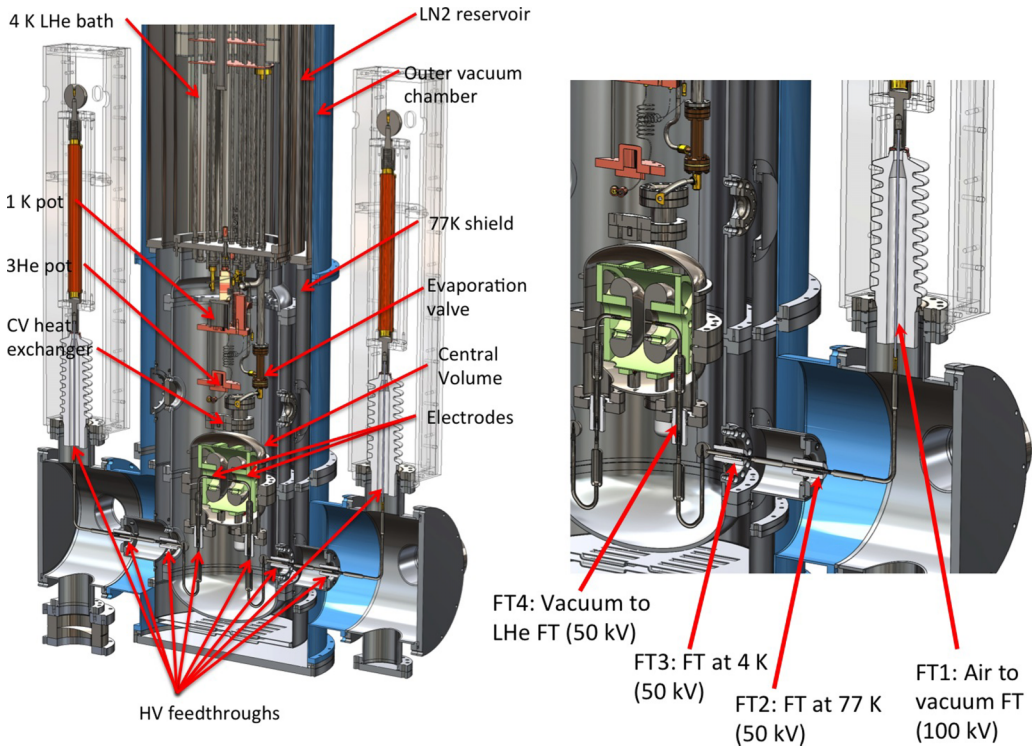

FIG. 2. A schematic of the MSHV system.

- LN_2 reservoir and the 77 K heat shield attached to it.
- 4 K LHe bath.
- Inner vacuum chamber (IVC), which also serves as a 4 K heat shield.
- ^{3}He refrigerator insert, which contains the ^{3}He pot and the 1K pot.
- The CV.
- HV feedthroughs and interconnects.

The dimension of the OVC is 50.8 cm in diameter and 185 cm in height. The IVC is made of 1100 series Al alloy for its excellent thermal conductivity. The IVC allows introduction of exchange gas to help cool the ^{3}He refrigerator insert and the CV in the process of cooldown.

A diagram of the plumbing of the MSHV system is shown in Fig. 3. The CV is cooled by the ^{3}He pot through a heat exchanger mounted at the bottom of the ^{3}He pot. The heat exchanger is made by cutting slots into a block of oxygen-free high thermal conductivity (OFHC) copper with electrical discharge machining.

There are two lines connected to the CV. One is the "fill" line, which connects the 4 K LHe bath to the CV through manual valve MV2, located at the bottom of the 4 K LHe bath. The primary purpose of the fill line is to introduce LHe into the CV. The fill line is thermally anchored at the 1 K pot. The other is the "pump out" line, which connects the CV to a vacuum pump through a large-aperture (6.35 mm) superfluid-tight valve MV1.[25] The primary purpose of the pump out line is to evacuate the CV prior to a cooldown of the system and remove LHe from the CV during a warmup of the system.

Opening MV2 allows LHe to flow from the 4 K LHe bath to the CV. Leaving it open keeps the pressure of the LHe inside the CV at the pressure of the LHe inside the 4 K LHe bath, which is typically 600 Torr, primarily determined by the atmospheric pressure in Los Alamos, New Mexico, USA (elevation ~2000 m). Note that there is a temperature gradient established in the LHe column inside the CV fill line, and the associated flow of heat to the CV, in this mode of operation. Closing MV2

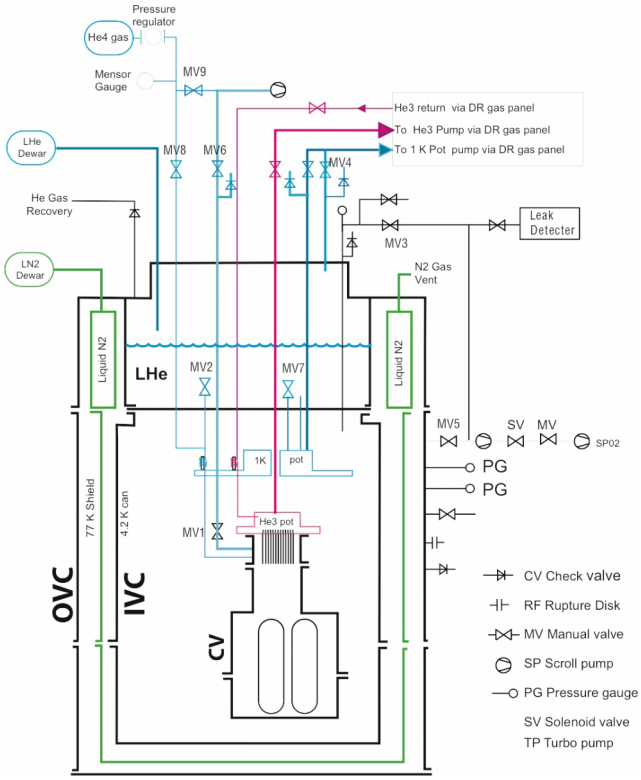

FIG. 3. MSHV plumbing diagram.

and pumping on the fill line to remove LHe from the fill line allow the pressure in the CV to be reduced. The pressure in the CV will be the SVP of LHe at the temperature at the location of the liquid surface, which is somewhere in the fill line. The diameter and length of the CV fill line were determined as a compromise between the following two competing factors:

- Heat flow rate. During operation, when the CV fill line is filled with LHe, there is a continuous flow of heat through the LHe from the 1 K pot to the CV, which is typically operated at 0.4 K. This must be sufficiently small so that it does not affect the temperature of the CV.
- He flow rate. The CV needs to be filled within a reasonable amount of time.

We evaluated the heat flow rate from 1.5 K to 0.4 K through a superfluid LHe column as a function of the diameter for selected lengths according to Ref. 26 using various thermodynamic quantities of LHe found in Ref. 27. Furthermore, we estimated the pressure drop necessary to have a sufficient flow to fill the CV in 24 h using formulas from Ref. 28. As a result of these evaluations, we chose the following for the length and the diameter of the fill line:

- LHe to 1 K pot: 47 cm long, 0.7 mm inner diameter.
- 1 K pot to CV: 76 cm long, 0.7 mm inner diameter.

The pump out line is ~6 mm in inner diameter. The large-aperture superfluid-tight valve is made of polyamide-imide.[25] The valve was mechanically actuated by using a rod, the other end of which is at room temperature. In order to properly thermally anchor the actuation rod to the 4 K shield, we used a solderless flexible thermal link.[29]

The CV, which houses the electrodes and holds about 6 l of LHe, is made of stainless steel. It is an ASME[30] stamped vessel with a maximum allowable working pressure of 8.6 bar (125 psi). The vessel is also equipped with a cryogenic burst disk[31] with a bursting pressure of 8.6 bar. This pressure rating of the CV was determined based on the following safety considerations. If the electricity to run the pumps for the ^{3}He is lost during the operation of the system, then the temperature of the CV will slowly rise and will remain at ~4 K as long as there is LHe in the 4 K LHe bath, as the CV is inside the 4 K heat shield. If the system is left unattended with MV2 closed, then the LHe inside the CV is confined and the pressure inside the CV will rise as the temperature of the CV rises. The pressure necessary to keep LHe in a fixed volume as the temperature rises is calculated to be ~7 bar (see the Appendix).

The CV can be opened at the 12-in. CF flange, allowing the electrodes to be replaced. The 12-in. CF flange with standard copper gasket provides a reliable superfluid LHe tight seal.

In addition to several temperature sensors, both silicon diodes and ruthenium oxide sensors, two LHe level sensors are installed inside the CV. One is a capacitance level sensor, which is made of two concentric cylinders mounted around the heat exchanger. This level sensor allows monitoring of the LHe level in the CV when the CV is close to being full. The dimensions of the cylinders are ~7 cm in height and ~4.5 cm in diameter. The gap between the inner and outer cylinders is 2.5×10^{-2} cm, giving a capacitance of ~300 pF. It is read out using a handheld LCR meter, Agilent Model U1733C, which provides more than sufficient resolution and accuracy to measure the change in capacitance caused by the dielectric constant of LHe (~1.05). The other LHe level sensor is of the superconducting wire type (American Magnetics, Inc., Model 135-2K). This level sensor provides the LHe level information during the initial fill and the emptying of the CV. Because the heat imparted to LHe when operating this sensor far exceeds the cooling power of the ^{3}He refrigerator, we keep this sensor turned off during normal operation.

A schematic showing the design of the CV, along with the location of some of the sensors, is shown in Fig. 4.

VI. DESIGN OF HV COMPONENTS

As mentioned earlier, there are two HV feed lines, each providing HV up to ±50 kV to the corresponding electrode. For each feed line, there are four HV feedthroughs. They are as follows:

- FT1: feedthrough to go from atmosphere to the insulating vacuum, located at room temperature.
- FT2: feedthrough to go through the 77 K shield. This feedthrough does not have to be leak tight. Its purpose is to thermally anchor the HV feed line to the 77 K shield.
- FT3: feedthrough to go through the IVC/4 K shield. This feedthrough needs to be vacuum tight as the IVC needs to hold the exchange gas.
- FT4: feedthrough to go from the IVC vacuum to LHe inside the CV. This feedthrough needs to be superfluid tight.

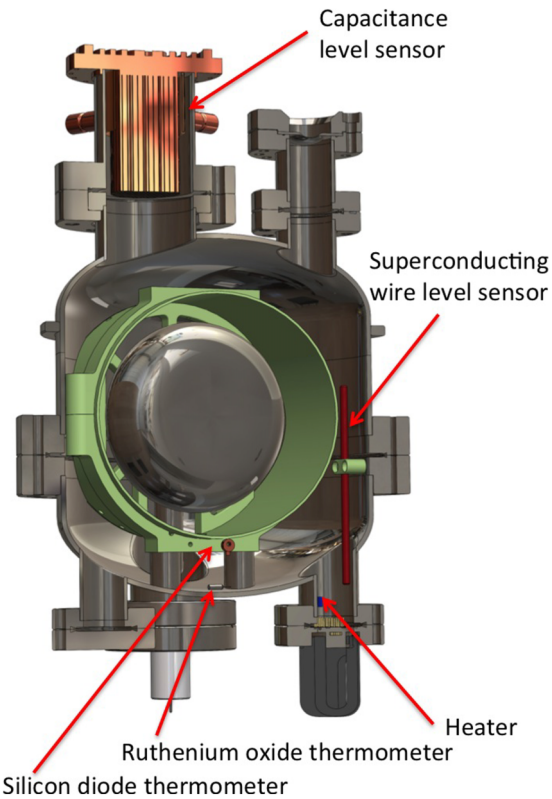

FIG. 4. The design of the CV, showing the locations of a capacitance level sensor, superconducting wire level sensor, and two thermometers.

There are also HV lines that connect between these feedthroughs.

Note that it is very important that heat leaks to the HV electrodes be minimized as they can cause vapor bubbles to be created on the surface of the electrodes, which in turn can initiate electrical breakdown, potentially leading to erroneous results, as mentioned earlier. The heat leaks to the HV electrodes were minimized by thermally anchoring the HV feed lines at each heat shield and by choosing a design and materials for the HV feed line that minimizes conductive heat leak.

A. HV feedthroughs

For FT1, we chose CeramTec[32] 100 kV feedthroughs (part no. 6722-01-CF). The reason for choosing 100 kV feedthroughs instead of 50 kV ones was the desire to be able to supply as high a potential as possible to each electrode. While the initial design goal was to achieve up to ±50 kV for the HV feed line for each electrode, the plan was to make improvements where possible.

For FT2, FT3, and FT4, due to spatial constraints, we chose CeramTec 50 kV feedthroughs (part no. 21183-01-W). This model is rated for use at 4 K. Prior to installing them in the MSHV apparatus, we performed measurements to characterize their performance for the following purposes:

- To determine the real performance limitation of these feedthroughs, as we are interested in applying as high a voltage as possible.
- To study how the performance of the feedthrough depends on the temperature, as some of the processes responsible for surface leakage currents and surface flashover may be suppressed at lower temperature.
- To study the dependence of the feedthrough performance on the method used to clean the ceramic.

We measured the (surface) leakage currents as a function of the voltage applied to the central conductor at 300 K and 77 K. Figure 5 shows a schematic of the apparatus used for this test.

Figure 6 shows results obtained at 300 K and 77 K for the following two methods of cleaning:

1. The feedthrough was first cleaned in an ultrasonic bath with Citranox, then cleaned with a plasma cleaner, and baked at 200 °C for 5 h.
2. The feedthrough was cleaned with a mixture of alumina powder and ethanol (purity >99.5%), rinsed with ethanol (purity >99.5%), and baked at 200 °C for 5 h.

The results indicate that the leakage current is smaller for 77 K than for 300 K. Also the performance of the feedthrough depends on the cleaning method employed. When the feedthrough was cleaned using the second method described above, it was possible to apply up to 90 kV with a leakage current less than 1 nA. All the feedthroughs used for FT2, FT3, and FT4 were prepared in this way prior to installation in the MSHV system.

B. HV interconnects

The HV lines connecting between the feedthroughs inside the cryostat need to meet the following requirements:

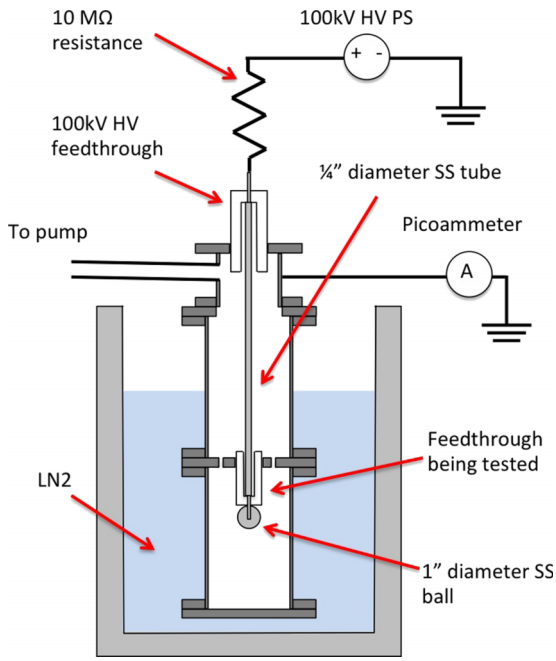

FIG. 5. A schematic of the apparatus used for the measurement of surface leakage currents of CeramTec 50 kV feedthroughs (part no. 21183-01-W) as a function of the voltage applied to the central conductor at 300 K and 77 K. The tested feedthrough was kept under vacuum.

- The conductive heat leak through the HV lines should be minimized.
- The HV lines need to have some amount of flexibility for installation and also for accommodating the thermal contraction of different parts of the system.
- The initial goal is to have a HV performance of $|V| \geq 50$ kV.

To meet these requirements, we settled on a design in which the HV lines are made of thin wall stainless steel tubing (6.35 mm diameter, 0.04 mm thick wall, 304 SS tubing) and formed bellows where flexibility is needed. Furthermore, a smooth metal sheath was slipped over each bellows section so as to avoid the ridges of the bellows causing high electric fields. The validity of such a design was confirmed using finite element electrostatic calculation, performed using COMSOL.[33] Additionally, the surface of the conductor was mechanically polished and was covered with Stycast 2850 FT Blue.

The design of the HV interconnecting line between FT3 and FT4 is shown in Fig. 7. Figure 8 shows a photograph of the bottom of the CV, which shows the HV lines from FT3 to FT4. The HV lines from FT4 to the electrodes were designed in a similar manner to the HV lines between the feedthroughs.

C. Power supply and HV resistor

We used two Model AF-100R0.1 100 kV DC HV power supplies from Matsusada Precision, Inc. HV was supplied to each HV feed line through a 1 GΩ HV resistor in order to limit the energy released inside the CV when an electrical breakdown occurs. The energy stored in the system is dominated by

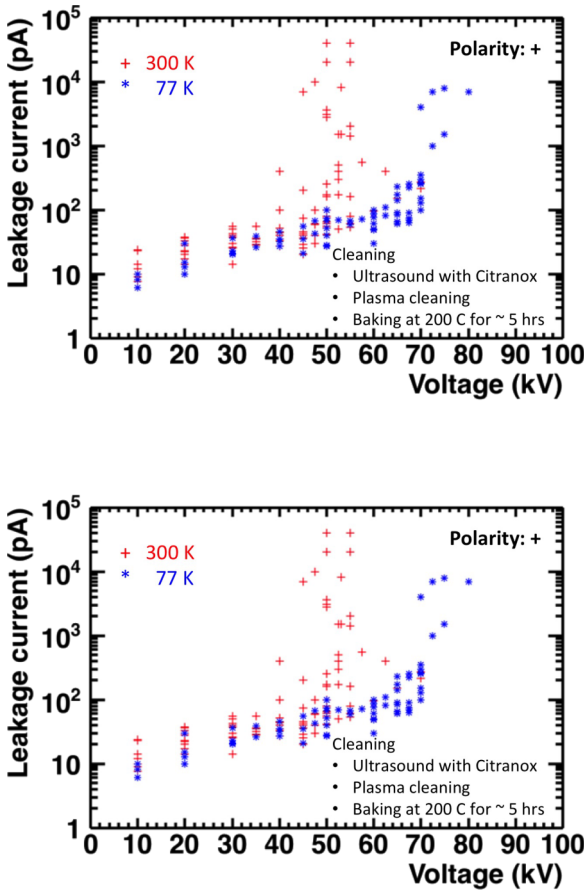

FIG. 6. Leakage currents measured for CeramTec 50 kV feedthroughs (part no. 21183-01-W) as a function of the voltage applied to the central conductor at 300 K and 77 K. Top: the feedthrough was first cleaned in an ultrasonic bath with Citranox, then was cleaned with plasma cleaner, and was baked at 200 C for 5 h. Bottom: the feedthrough was cleaned with a mixture of alumina powder and ethanol (purity >99.5%), then was rinsed with ethanol (purity >99.5%), and then was baked at 200 C for 5 h.

that stored in the room temperature HV cable connecting the power supply to the MSHV system, which has a capacitance of ~300 pF. Therefore, the HV resistance was placed between FT1 and the room temperature HV cable.

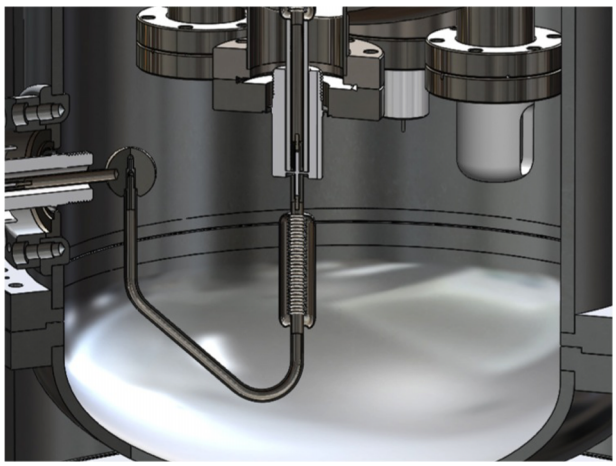

FIG. 7. The design of the HV interconnecting line between FT3 and FT4.

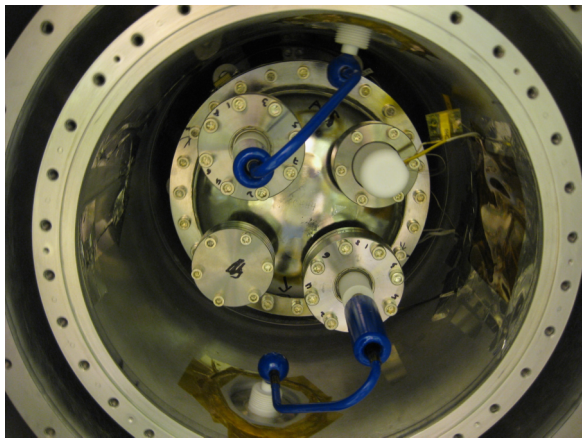

FIG. 8. Photograph of the bottom of the CV, which shows the HV lines from FT3 to FT4.

D. Rogowski electrodes

The goal of the initial HV test was to establish the electric field strength that is possible with an electrode material known to be capable of good performance. Therefore, the initial electrodes were made of electropolished stainless steel. Stainless steel is one of the materials that are known to give higher breakdown fields than others.

For the shape of the electrodes, we chose the so-called Rogowski profile,[34] which provides a uniform electric field in the gap and ensures that the gap has the highest field in the system. Figure 9 shows a result of a finite element electrostatic calculation, performed using COMSOL,[33] of the Rogowski electrodes that we used. We also performed finite element electrostatic calculations for other known uniform field electrode (UFE) shapes, such as that by Chang[35] and that by Ernst.[36] We did not see a significant difference among these UFE shapes in terms of the uniformity of the electric field in the gap and of the area over which the field is uniform. For the chosen geometry, the field is uniform to 2% over ~64 cm^2.

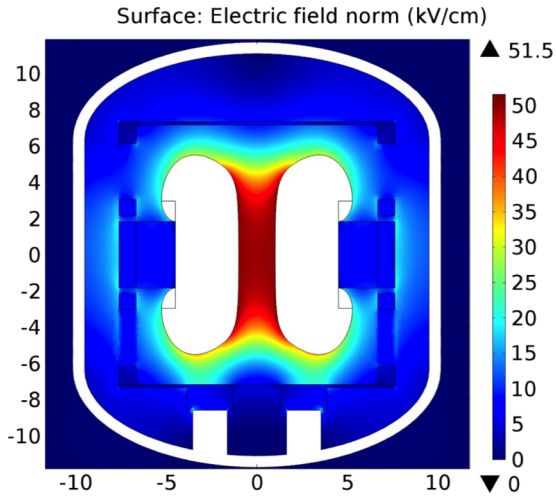

FIG. 9. Result of a finite element electrostatic calculation, performed using COMSOL,[33] of the Rogowski electrodes mounted inside the CV. For this calculation, the gap between the two electrodes was set to 2 cm and the two electrodes were held at +50 kV and −50 kV.

We decided to electropolish the electrodes based on the following considerations. A protrusion on the electrode surface would cause a spot with higher electric field (a "hot spot"). The strength of the field on such a hot spot does not depend on the size of the protrusion but on its shape, as long as the size of the protrusion is much smaller than the distance between two electrodes. For example, if a half-sphere is embedded on a surface of a flat electrode that forms a parallel plate capacitor and the field between the two plates is E_0 in the absence of the half-sphere, then the field on the top of the half-sphere is $3E_0$, regardless of the size of the half-sphere, as long as the radius r of the sphere is much smaller than the distance d between the two plates.[37] The lack of dependence of the field strength on the size of the sphere can be easily understood by realizing that there is no length scale in the problem when $r \ll d$. It follows that the amount of the field strength enhancement due to features on the electrode surface depends on the shape of the features but not on the size. Surface smoothness is typically expressed in terms of the size of the features on the surface and mechanical polishing processes reduce the size of the features. However, it is not the relevant quantity in this case. Electropolishing on the other hand is expected to make the shape of the features smoother. For this reason, we decided to electropolish the first set of electrodes, although the difference between electropolished surfaces and machine polished surfaces needs to be ultimately studied experimentally.

Figure 10 shows how the electrodes were mounted inside the CV. The electrodes were supported by a "cage" made of fiberglass-reinforced plastic (FRP), in this case, G-10. A spacer ring made of FRP was bolted onto the back of each electrode with a set of unfilled Torlon bolts. The spacers were then mounted onto the end caps of the FRP cage using Torlon bolts. With such a supporting structure, the electrodes were expected to remain parallel to each other to ~0.1° when cooled. With the aid of COMSOL-based electrostatic calculations, we determined that with the expected tolerance within which the two electrodes can be located, the effect of possible misalignment (both angular and translational) of the electrodes on the field uniformity and the area over which the field is uniform would be insignificant. The effect of the supporting structure on the electric field distribution was also evaluated as shown in Fig. 9. The HV lines were included in the electrostatic modeling to see the strength of the field on the surface.

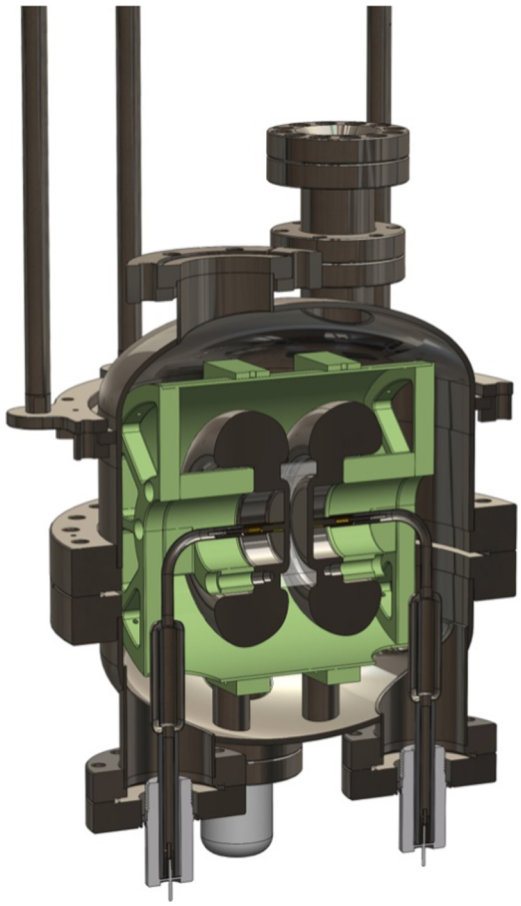

FIG. 10. An image showing how the electrodes were supported inside the CV. The grooved electrodes with a PMMA ring are shown.

E. Grooved electrodes

The second test we performed was to study the effect of having a dielectric object sandwiched between two electrodes. As indicated earlier, it is well known that when a dielectric object is inserted between two electrodes, the holdoff voltage is reduced, which is thought to be due to field emission at the cathode-insulator junction and emitted electrons running along the insulator surface.[24] A traditional solution to this problem is to embed the end of the insulator into a groove.[23,24] The idea is to "hide" the edges of the insulator in a low field region to avoid the enhancement of the field at the cathode-insulator junction due to the higher dielectric constant of the dielectric. Designs in which the insulator surface is at 45° with respect to the flat electrode surface are also used, in particular for pulsed high-power high-voltage applications.[38] However the latter method is not suitable for our application.

We used a PMMA cylinder 6.35 cm in OD and 5.08 cm in ID as our dielectric insert. We designed a set of electrodes with a groove with the help of finite element electrostatic analysis using COMSOL.[33] Figure 11 shows results from such electrostatic calculations. The shape of the groove was adjusted so that the highest field in the system, which occurs on the rounded corner of the groove, is less than ~1.15 times the uniform field in the middle of the electrodes with and without the dielectric insert. We started with a groove 5.5 mm deep and 8.4 mm wide (2 mm larger than the insulator's wall thickness), and adjusted the shape of the edge of the groove by trial and error using COMSOL's chamfer and fillet tools in order to achieve the necessary field profile. In doing so, the following competing factors were taken into consideration:

1. If the rounding of the edge of the groove has too small a radius, then there will be a high field region between the rounded edge of the groove and the side wall of the PMMA insert. Whereas the surface of the electrode, including the rounded edge of the groove, forms an equipotential surface, there is a potential gradient along the surface of the PMMA insert. Therefore, the distance between the electrode surface and the PMMA insert surface being too

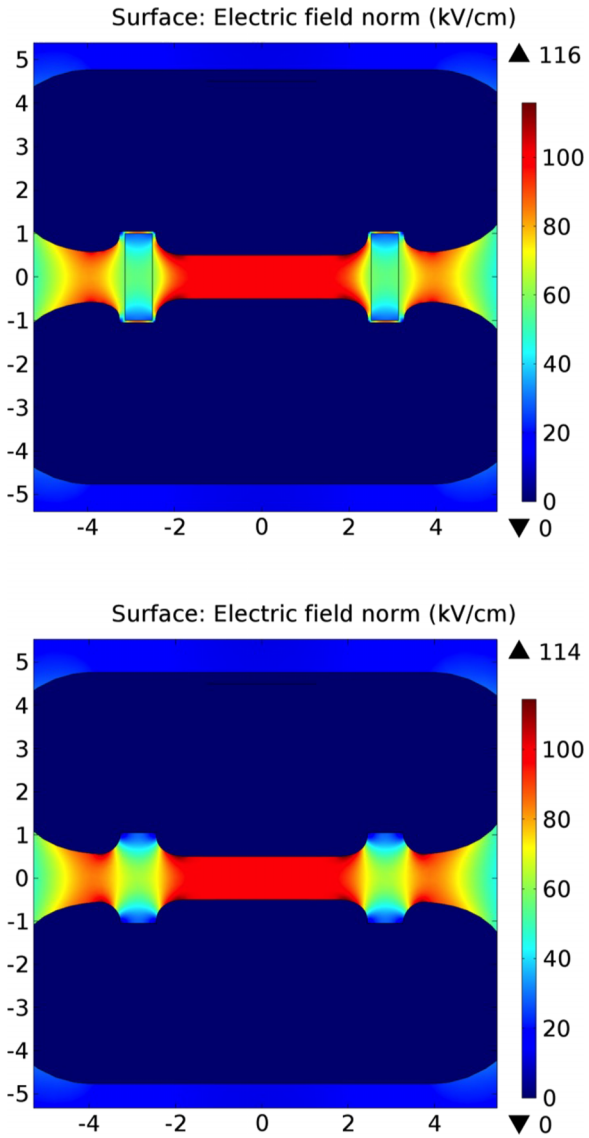

FIG. 11. Electrostatic models of the grooved electrodes. Top: with the PMMA insert. Bottom: without the PMMA insert. For these calculations, the gap between the two electrodes was set to 1 cm and the two electrodes were held at +50 kV and −50 kV.

close at the location of the rounded edge of the groove causes the field there to be high.

2. If the rounding of the edge of the groove has too large a radius, then the field at the bottom of the groove does not become sufficiently low.

Figure 12 shows photographs of the grooved electrodes and the PMMA insert.

VII. CRYOGENIC PERFORMANCE AND OPERATIONAL EXPERIENCE

At the time of this writing, the system has been operated 18 times successfully. In this section, we describe the cryogenic performance of the system and our operational experience with the system. As mentioned earlier, one of the design goals was to achieve a turnaround time of 2 weeks. We have demonstrated that indeed turning around the system in two weeks was possible, including the time to replace the contents of the CV.

FIG. 12. Photographs of the grooved electrodes and the PMMA insert.

A. Cooldown and temperature control

The cooldown of the system starts with precooling the LHe bath with liquid nitrogen (LN_2) as is done as a standard practice for many LHe cryostats. In doing so, the IVC is filled with 1 atm N_2 gas as the exchange gas to cool the 1 K pot, the ^{3}He pot, and the CV. Once the system reaches LN_2 temperature, which takes ~12 h after the LHe bath is filled with LN_2, the remaining LN_2 is removed from the LHe bath and the N_2 exchange gas is pumped out of the IVC volume.

The system is further cooled by transferring LHe (initially cold helium gas) to the LHe bath. During this time, the CV is cooled by opening both MV1 and MV2 and flowing LHe (initially cold helium gas) from the LHe bath through the CV. The 1 K pot is also pumped on at the same time. As the CV is cooled sufficiently, the CV gets filled with LHe. It takes approximately 6 h for the CV to become completely filled from the time when LHe starts to accumulate at the bottom of the CV. Once the CV becomes completely filled with LHe, MV1 is closed. When the CV becomes full, the temperature of the CV is ~1.8 K. We also tried filling the IVC with helium gas as the exchange gas to cool the CV, instead of flowing cold helium gas through the CV. We found that flowing cold helium gas and LHe through the CV is a more efficient way of cooling it

than using an exchange gas, because the use of exchange gas required spending time in pumping out the exchange gas.

The ^{3}He refrigerator is then turned on and the ^{3}He circulation starts. This further cools the CV. It takes approximately 4 h to reach 0.4 K. Overall, it takes ~2.5 days to go from the CV being empty at 300 K to the CV being filled with 0.4 K LHe.

The temperature of the CV can easily be controlled either by adjusting the ^{3}He circulation or by using heaters that are mounted inside the CV (directly in contact with LHe) and on the outside wall of the CV.

B. Pressure control and monitoring

As mentioned earlier, leaving MV2 open keeps the pressure of the LHe inside the CV at the pressure of the LHe inside the 4 K LHe bath, which is typically 600 Torr. Closing MV2 and pumping on the fill line to remove LHe from the fill line allow the pressure in the CV to be reduced. The pressure can be increased by stopping pumping on the fill line and opening MV2 momentarily. The pressure in the CV will be the SVP of LHe at the temperature at the location of the liquid surface, which is somewhere on the fill line, along which there is a temperature gradient. The pressure can be changed and controlled with ease between ~1 Torr and ~600 Torr with the method described above. Going below ~1 Torr cannot be achieved efficiently by simply pumping on the fill line, because the vapor pressure of helium becomes smaller and smaller. However, lower pressures can be achieved by removing LHe from the fill line by first warming up the CV while pumping on the fill line and cooling it again. Warming up the CV to higher temperatures makes it easy to remove LHe from the fill line because of the higher vapor pressure. Note that the hydrostatic pressure of LHe is ~0.1 Torr/cm. Therefore even if the LHe surface is below the top of the CV, in which case the lowest pressure inside the CV is $\sim 10^{-6}$ Torr, the pressure at the location of the electrodes is ~1 Torr.

The pressure inside the CV can be monitored by the external pressure gauge (Mensor model 2101), as indicated in Fig. 3. In addition, the pressure change inside the CV can be monitored using the capacitance LHe level sensor mounted around the heat exchanger. The change in the dielectric constant due to the change in pressure is large enough to make the capacitance level sensor sensitive to the pressure change. The dielectric constant ϵ is related to the density ρ via the Clausius-Mossotti relation

$$\frac{\epsilon - 1}{\epsilon + 2} = \frac{4\pi\alpha_M\rho}{3M}, \tag{2}$$

or solving for ϵ,

$$\epsilon = \frac{1 + 2\eta}{1 - \eta}, \qquad \eta = \frac{4\pi\alpha_M\rho}{3M}, \tag{3}$$

where M is the molecular weight and α_M is the molar polarizability. The density ρ depends on the pressure and temperature. α_M has a very weak pressure dependence. Since $\eta \ll 1$ and the density increases approximately linearly with the pressure in the pressure range we are interested in ($p \lesssim 1$ atm), it is expected that the value of ϵ and therefore the capacitance of the LHe level sensor depends approximately linearly on the pressure.

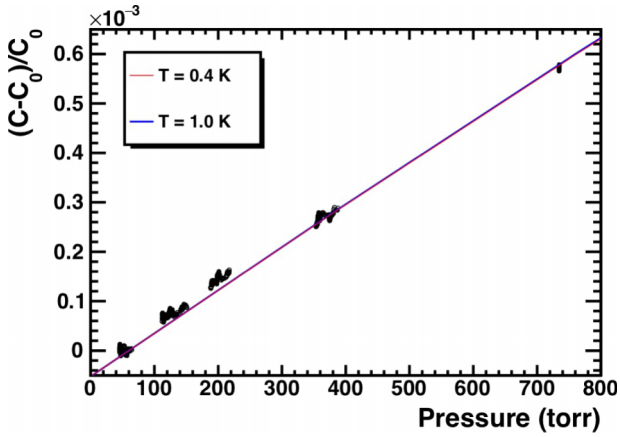

FIG. 13. The measured capacitance output of the LHe level sensor plotted as a function of the pressure of LHe inside the CV as measured by an external pressure gauge. C_0 refers to the capacitance measured at the reference pressure, which in this case was 60 Torr. Also shown is the expected change in capacitance as a function of pressure, calculated from Eq. (3) using molar volume data from Ref. 39 and assuming a constant α_M from Ref. 40 for two different temperatures, illustrating insensitivity to temperature in this range.

In Fig. 13, the measured change in capacitance is plotted as a function of the pressure as measured by the external pressure gauge and is compared to what is expected from Eq. (3) with molar volume data from Ref. 39 and assuming a constant α_M from Ref. 40. The relative change in capacitance is plotted, rather than the value of the dielectric constant, because we do not have sufficiently accurate information on the geometry of the capacitor to extract the value of the dielectric constant from the measured capacitance. However, these results demonstrate that the capacitance level LHe meter serves as an internal pressure gauge with precision sufficient for our purpose.

C. Removal of LHe and warming up

When warming up the system, LHe from the CV can be removed by opening MV1, pumping on the CV, and turning on the heater in the CV, after stopping the ^{3}He circulation. With a heater power of ~0.6 W, it takes ~8 h to remove LHe from the CV. By spoiling the insulation vacuum with clean neon gas after all the cryogen is removed from the system, the system can be warmed up to room temperature in ~2 days.

VIII. HV PERFORMANCE, OPERATIONAL EXPERIENCE, AND INITIAL RESULTS

A. Holdoff voltage

For the initial HV tests, we operated the HV power supplies manually. Typically we increased the HV at a rate of 0.5 kV/s or less pausing every 5 or 10 kV. The current monitor output of the power supplies, which gives a 10 V output for a 0.1 mA current, was connected to a digital oscilloscope for monitoring and recording. Electrical breakdown events with currents of ~0.1 μA were easily detected. Initial tests indicated that the performance of the HV feedlines was limited to approximately ±40–50 kV. Applying a higher voltage causes

breakdown from the HV feedline to the ground. Likely locations for this are inside the CV.

For neither of the two electrode configurations discussed in Secs. VI D and VI E was electrical breakdown between the two electrodes observed. In both cases, the applicable HV was limited by the performance of the HV feedlines. For the case of the electropolished stainless steel Rogowski electrodes, we were able to stably apply up to 105 kV across the 1 cm gap for a wide range of pressures and temperatures. For the electropolished stainless steel electrodes with a groove, we were able to stably apply up to 80 kV across the 1 cm gap for a wide range of pressures and temperatures, with and without the PMMA insert. Note that the HV feedlines inside the CV were different between these two cases, because of the slightly different design of the back of the electrodes. These initial results are summarized in Table I.

B. Leakage currents

As discussed in the Introduction, in the SNS nEDM experiment the leakage currents along the cell walls need to be minimized. Processes responsible for leakage currents may be suppressed at cryogenic temperatures. It is therefore important to study the leakage currents when a dielectric object is sandwiched between two electrodes in the MSHV system.

As a first step, we measured the current flowing between the two electropolished stainless steel Rogowski electrodes (i.e., no dielectric objects between two electrodes). The measurement was done by applying HV to one electrode and measuring the current coming out of the other electrode using a picoammeter. In this configuration, the maximum voltage difference between the two electrodes was half of that possible when both electrodes are connected to the respective HV power supply. The reason for doing this is that the leakage current through the surface of the feedthrough insulators and that through the insulator of the room temperature HV cables are much larger than the current expected to flow between the two electrodes.

The measured current was less than 1 pA with 45 kV applied to one of the electrodes. The measurement was limited by the sensitivity of the current measuring device. This gives a lower bound on the effective volume resistivity of LHe of $\rho_V > 5 \times 10^{18}\ \Omega$ cm. This lower bound is 5 times larger than the bound given in Ref. 41. Note that the current flowing in LHe due to charge generated by cosmic rays was estimated to be $I_c \sim 10^{-14}$ A, smaller than the experimentally obtained limit by two orders of magnitude. The contribution from the natural radioactivity was also estimated to be $I_r \sim 10^{-14}$ A, based on a measurement of the radioactivity on the surface of the electrodes.

TABLE I. Summary of holdoff voltage results. Note that in all cases except noted, the gap between the electrodes was 1 cm and the highest achievable stable field was limited by the performance of the HV feedlines.

Configuration	Temperature (K)	Pressure (Torr)	Highest achievable stable field (kV/cm)
SS Rogowski electrodes	2.5-2.8	72, 90, 785	90
SS Rogowski electrodes	1.1	13	90
SS Rogowski electrodes	0.42	SVP, 664	105
SS electrodes with a groove without the PMMA insert	2.7	620	70
SS electrodes with a groove without the PMMA insert	0.5	1.0, 620	80
SS electrodes with a groove with the PMMA insert	2.1	614	50[a]
SS electrodes with a groove with the PMMA insert	0.5	SVP, 2.7, 574	80

[a]Higher voltages were not tried.

IX. SUMMARY AND OUTLOOK

We have designed, constructed, commissioned, and operated an apparatus for studying electrical breakdown in liquid helium at 0.4 K and testing electrode materials for the SNS nEDM experiment. It can cool a 6 l liquid helium volume, which holds a set of electrodes, to 0.4 K. The pressure of the LHe inside this volume can be varied between the saturated vapor pressure and ~600 Torr. High voltage up to ±50 kV can be applied to each electrode. This apparatus can be operated to perform two successive cooldowns two weeks apart. Initial results have demonstrated that it is possible to apply fields exceeding 100 kV/cm in a 1 cm gap between two electropolished stainless steel electrodes 12 cm in diameter for a wide range of pressures. In addition, it has been demonstrated that fields exceeding 80 kV/cm can be applied in a 1 cm gap between two electropolished stainless steel electrodes 12 cm in diameter with a dielectric insert sandwiched between the electrodes with a properly designed groove to accommodate the insert. In both cases the applicable fields were limited by the performance of the HV feedlines.

ACKNOWLEDGMENTS

This work was supported by the United States Department of Energy Office of Nuclear Physics. Development of acrylic-substrate electrodes was supported by the Laboratory Directed Research and Development (LDRD) of Oak Ridge National Laboratory. We gratefully acknowledge the support of Physics and AOT Divisions as well as the former LANSCE Division of Los Alamos National Laboratory. We also are grateful to Brown University Physics Department for making the ^{3}He refrigerator and the cryostat available for this effort. One of the authors (T.M.I.) expresses his gratitude to Dr. M. Hardiman of the University of Sussex for fruitful discussions.

APPENDIX: TEMPERATURE DEPENDENCE OF THE PRESSURE OF LIQUID HELIUM IN A CONFINED CONTAINER

Since the thermodynamic properties of liquid helium are well known,[27,42–44] it is straightforward to calculate the temperature dependence of the pressure of a confined volume

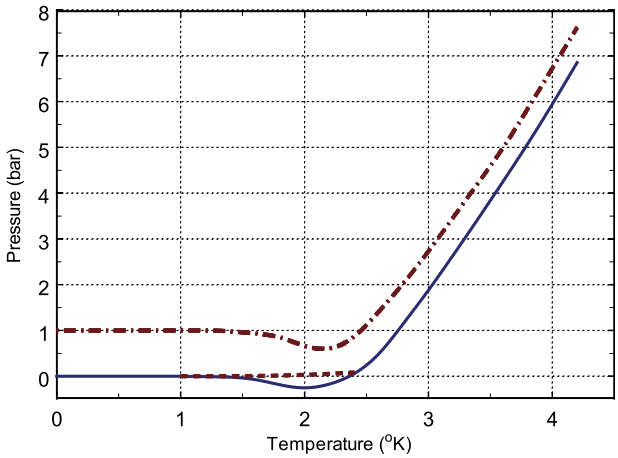

FIG. 14. Pressure of confined liquid helium plotted as a function of the temperature. *Solid and dashed lines:* the cell sealed at 1 K at the saturated vapor pressure (see text for details). *Dotted-dashed line:* the cell sealed at 1 K at a pressure of 1 bar.

of the liquid. The result of such a calculation is shown in Fig. 14 for the liquid sealed at 1 K. The solid curve is the pressure of the helium sealed at 1 K at the saturated vapor pressure if it were not to cavitate when the pressure becomes negative. In the temperature range between 1.15 K and the lambda point where the thermal expansion of the liquid is negative, the contained helium develops a vapor phase and the pressure follows the dashed saturated vapor pressure line in Fig. 14. Above 2.2 K the pressure within the container rises monotonically with temperature reaching about 7 bar at 4.2 K. The dotted-dashed curve is the pressure of the helium sealed 1 K at a pressure of 1 bar.

[1]J. H. Smith, E. M. Purcell, and N. F. Ramsey, Phys. Rev. **108**, 120 (1957).
[2]S. K. Lamoreaux and R. Golub, J. Phys. G: Nucl. Part. Phys. **36**, 104002 (2009).
[3]V. K. Ignatovich, *The Physics of Ultracold Neutrons* (Clarendon, Oxford, 1990).
[4]R. Golub, D. Richardson, and S. K. Lamoreaux, *Ultra-Cold Neutrons* (Adam Hilger, Bristol, 1991).
[5]F. M. Piegsa, Phys. Rev. C **88**, 045502 (2013).
[6]C. A. Baker *et al.*, Phys. Rev. Lett. **97**, 131801 (2006).
[7]J. M. Pendlebury *et al.*, Phys. Rev. D **92**, 092003 (2015).
[8]N. Fomin, G. L. Greene, R. R. Allen, V. Cianciolo, C. Crawford, T. M. Ito, P. R. Huffman, E. B. Iverson, R. Mahurin, and W. M. Snow, Nucl. Instrum. Methods Phys. Res., Sect. A **773**, 45 (2015).
[9]The nEDM experiment (B. W. Filippone, spokesperson), http://p25ext.lanl.gov/edm/edm.html.
[10]T. M. Ito, J. Phys.: Conf. Ser. **69**, 012037 (2007).
[11]R. Golub and S. K. Lamoreaux, Phys. Rep. **237**, 1 (1994).
[12]R. Golub and J. M. Pendlebury, Phys. Lett. A **62**, 337 (1977).
[13]T. M. Ito, S. M. Clayton, J. Ramsey, M. Karcz, C.-Y. Liu, J. C. Long, T. G. Reddy, and G. M. Seidel, Phys. Rev. A **85**, 042718 (2012).
[14]P. Ageron, W. Mampe, and A. L. Kilvington, Z. Phys. B **59**, 261 (1985).
[15]E. Korobkina, R. Golub, J. Butterworth, P. Geltenbort, and S. Arzumanov, Phys. Rev. B **70**, 035409 (2004).
[16]J. Gerhold, Cryogenics **38**, 1063 (1998).
[17]A. A. Belevtsev, Nucl. Instrum. Methods Phys. Res., Sect. A **327**, 18 (1993).
[18]R. Kattan, A. Denat, and O. Lesaint, J. Appl. Phys. **66**, 4062 (1989).
[19]E. F. Kelly and R. E. Hebner, Jr., J. Appl. Phys. **52**, 191 (1981).
[20]E. O. Foster, J. Phys. D: Appl. Phys. **23**, 1506 (1990).
[21]F. A. M. Rizk and G. N. Trinh, *High Voltage Engineering* (CRC Press, Boca Raton, 2014), Chap. 6.
[22]K. H. Weber and H. S. Endicott, Trans. Am. Inst. Electr. Eng. **75**, 371 (1956).
[23]R. Golub, Sov. Phys. Tech. Phys. **31**, 945 (1986).
[24]M. J. Kofoid, Trans. Am. Inst. Electr. Eng. **79**, 999 (1960).
[25]S. E. Williamson *et al.*, "Large-aperture, non-magnetic, superfluid-tight valves" (unpublished).
[26]B. Bertman and T. A. Kitchens, Cryogenics **8**, 36 (1968).
[27]R. J. Donnelly and C. F. Barenghi, J. Phys. Chem. Ref. Data **27**, 1217 (1998).
[28]H. A. Snyder and A. J. Mord, J. Low Temp. Phys. **86**, 177 (1992).
[29]Space Dynamics Laboratory, http://www.sdl.usu.edu.
[30]The American Society of Mechanical Engineering, http://www.asme.org.
[31]OSECO, http://www.oseco.com.
[32]CeramTec North America Corp., http://www.ceramtec.us.
[33]COMSOL Multiphysics, http://www.comsol.com.
[34]J. D. Cobine, *Gaseous Conductors: Theory and Engineering Applications* (McGraw Hill, 1958).
[35]T. Y. Chang, Rev. Sci. Instrum. **44**, 405 (1973).
[36]G. J. Ernst, Opt. Commun. **47**, 47 (1983).
[37]R. Le Ny, J. Phys. A: Math. Gen. **14**, 945 (1981).
[38]W. A. Stygar *et al.*, Phys. Rev. Spec. Top.–Accel. Beams **8**, 050401 (2005).
[39]E. Tanaka, K. Hatakeyama, S. Noma, and T. Satoh, Cryogenics **40**, 365 (2000).
[40]R. F. Harris-Lowe and K. A. Smee, Phys. Rev. A **2**, 158 (1970).
[41]C. Blank and M. H. Edwards, Phys. Rev. **119**, 50 (1960).
[42]D. L. Elwell and H. Meyer, Phys. Rev. **164**, 245 (1967).
[43]R. D. McCarty, J. Phys. Chem. Ref. Data **2**, 923 (1973).
[44]J. Maynard, Phys. Rev. B **14**, 3868 (1976).